Molecular Therapy
Original Article

The Role of MicroRNA-21 in Venous Neointimal Hyperplasia: Implications for Targeting miR-21 for VNH Treatment

Sreenivasulu Kilari,[1] Chuanqi Cai,[1,2] Chenglei Zhao,[1,3] Amit Sharma,[1] Ekaterina Chernogubova,[4] Michael Simeon,[1] Chin-Cheng Wu,[5] Hsiang-Lin Song,[6] Lars Maegdefessel,[4] and Sanjay Misra[1,7]

[1]Vascular and Interventional Radiology Translational Laboratory, Department of Radiology, Mayo Clinic, Rochester, MN, USA; [2]Department of Vascular Surgery, Union Hospital, Tongji Medical College, Huazhong University of Science and Technology, Wuhan, China; [3]Department of Vascular Surgery, The Second Xiangya Hospital, Central South University, Changsha, Hunan, China; [4]Molecular Medicine and Surgery, Karolinska Institute, Stockholm, Sweden; [5]Cardiovascular Center, National Taiwan University Hospital, Hsinchu Branch, Taiwan; [6]Pathology Department, National Taiwan University Hospital, Hsinchu Branch, Taiwan; [7]Department of Biochemistry and Molecular Biology, Mayo Clinic, Rochester, MN, USA

The molecular mechanism of hemodialysis access arteriovenous fistula (AVF) failure due to venous neointimal hyperplasia (VNH) is not known. The role of microRNA-21 (miR-21) in VNH associated with AVF failure was investigated by performing *in vivo* and *in vitro* experiments. *In situ* hybridization results revealed that miR-21 expression increased and was associated with fibroblasts in failed AVFs from patients. In a murine AVF model, qRT-PCR gene expression results showed a significant increase in miR-21 and a decrease in miR-21 target genes in graft veins (GVs) compared to contralateral veins in mouse AVF. miR-21 knockdown in GVs was performed using a lentivirus-mediated small hairpin RNA (shRNA), and this improved AVF patency with a decrease in neointima compared to control GVs. Moreover, loss of miR-21 in GVs significantly decreased the *Tgfβ1*, *Col-Ia*, and *Col-Iva* genes. Immunohistochemistry demonstrated a significant decrease in myofibroblasts and proliferation with an increase in terminal deoxynucleotidyl transferase dUTP nick-end labeling (TUNEL) staining in miR-21-knockdown vessels, along with a decrease in hypoxia-inducible factor-1 alpha (HIF-1α) and phospho-SMAD2 (pSMAD-2) and phospho-SMAD3 (pSMAD-3) and an increase in phosphatase and tensin homolog (PTEN) staining. Hypoxic fibroblast knockdown for miR-21 showed a significant decrease in *Tgfβ-1* expression and pSMAD-2 and -3 levels and a decrease in myofibroblasts. These results indicate that miR-21 upregulation causes VNH formation by fibroblast-to-myofibroblast differentiation.

INTRODUCTION

More than 2.3 million patients are affected by end-stage renal disease worldwide, and the majority of them require hemodialysis through a well-functioning vascular access, with arteriovenous fistula (AVF) being the gold standard. AVFs are prone to venous neointimal hyperplasia (VNH) resulting in venous stenosis.[1] It is hypothesized that hypoxic (Hyp) injury to the vasa vasorum at the time of AVF placement could trigger VNH formation through the proliferation and migration of fibroblasts and vascular smooth muscle cells and matrix deposition.[2] Excitingly, microRNA-21 (miR-21) contributes to fibrogenic activation and fibroblast-to-myofibroblast differentiation,[3] and miR-21 dysregulation has been observed in vein graft failure of a coronary bypass graft model.[4] Moreover, *in vitro* studies revealed that miR-21 upregulation increased fibroblast proliferation.[5] This could be an early critical step in the pathogenesis of VNH.

In this study, we found that there was an increased expression of miR-21 in failed AVF samples removed from patients and that miR-21 was localized to the intima and media regions where fibroblasts accumulated. Expression of miR-21 was significantly upregulated with AVF creation, accompanied by an increase in profibrotic genes in the outflow veins of AVF in a murine model with chronic kidney disease. Knockdown of miR-21 using lentivirus-mediated small hairpin RNA (shRNA) transduction to the outflow vein of the murine AVF model resulted in a significant decrease in the neointima area and ratio of neointima to media plus adventitia, in association with decreases in cell proliferation, smooth muscle, and myofibroblasts. Furthermore, *in vitro* cell culture studies demonstrated that the loss of miR-21 attenuated Hyp-induced fibroblast-to-myofibroblast differentiation via SMAD2/3 signaling in mouse pulmonary vein fibroblasts.

RESULTS

miR-21 Expression Is Increased in Stenotic Veins of Patient AVFs

We used venous tissue samples from patients with stenosis formation and those undergoing placement of an AVF.[6,7] *In situ* hybridization (ISH) for miR-21 demonstrated that miR-21 expression was

Received 25 November 2018; accepted 19 June 2019;
https://doi.org/10.1016/j.ymthe.2019.06.011.

Correspondence: Sanjay Misra, MD, FSIR, FAHA, Vascular and Interventional Radiology Translational Laboratory, Department of Radiology, Mayo Clinic, 200 First Street SW, Rochester, MN 55905, USA.
E-mail: misra.sanjay@mayo.edu

This is an open access article under the CC BY-NC-ND license (http://creativecommons.org/licenses/by-nc-nd/4.0/).

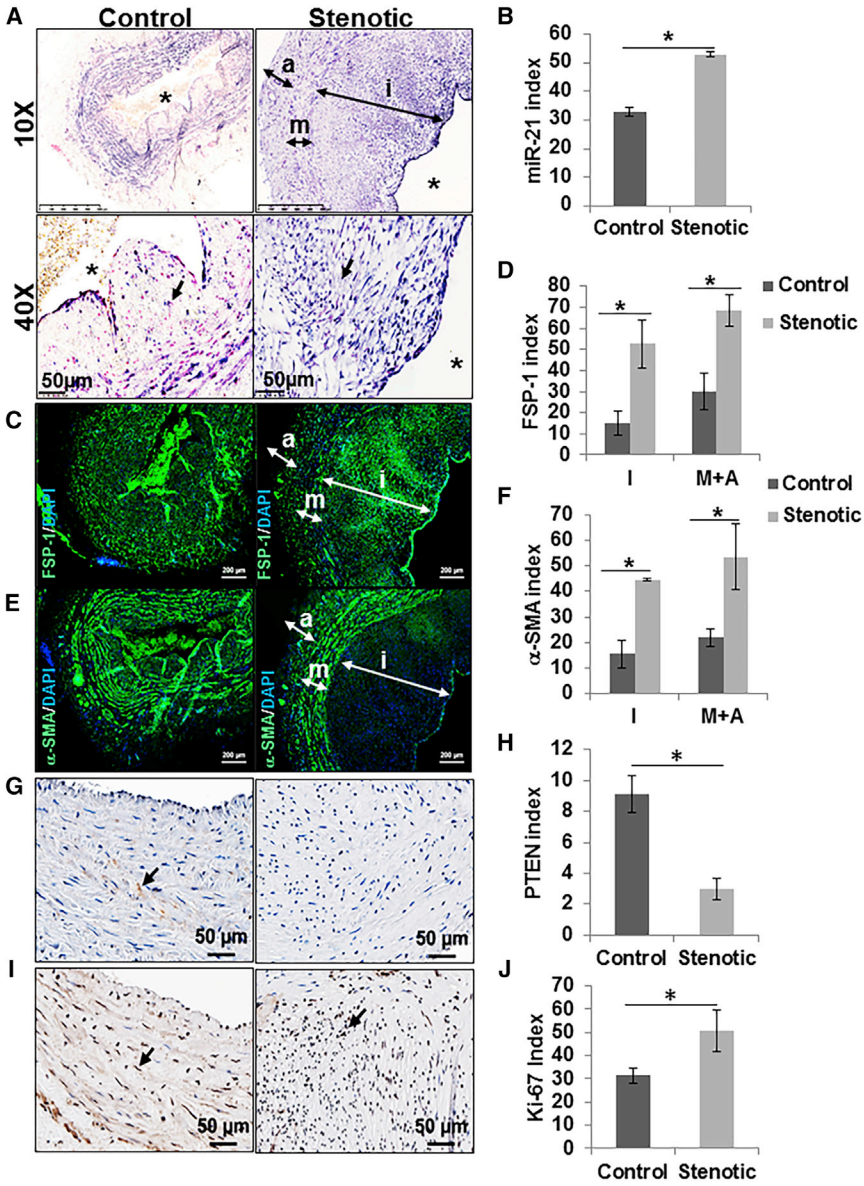

Figure 1. AVF Creation Induces miR-21 Expression Predominantly in Cells Staining Positive for FSP-1

(A) *In situ* hybridization for miR-21 expression levels in outflow vein segments of functional (control) and failed (stenotic) AVF specimens of the same patient. Arrows show cells staining positive for miR-21 transcript have a purple color with nuclei stained red. The images in the upper panel (scale bar, 500 μm) are digitally enlarged and shown in the lower panel (scale bar, 50 μm). (B) The mean intensity of the purple color staining (miR-21 index) was measured as described. Immunofluorescence staining for (C) fibroblast-specific protein (FSP)-1 and (E) α-smooth muscle cell actin (α-SMA). Cells with cytoplasm stained green are positive for FSP-1 and α-SMA. FSP-1(+) cells localized to the intima and α-SMA(+) cells to the media and adventitia. The intensities of (D) FSP-1-positive and (F) α-SMA-positive green cell distribution between intima and media plus adventitia layers are shown in the bar graph. Representative images were obtained at 20× magnification of (G) PTEN and (I) Ki-67 staining. The arrows point to brown-stained cells that are positive for (G) PTEN and (I) Ki-67. The bar graphs represent the mean intensity of chromogen staining (H) PTEN and (J) Ki-67 staining. The data points in the bar graph are represented as the mean ± SEM. *$p < 0.05$. Different layers of vessel wall are indicated with double-headed arrows. a, adventitia; m, media; i, intima.

significantly increased in stenotic samples compared to non-stenotic samples (Figures 1A and 1B). Since smooth muscle and fibroblasts are present in the venous stenosis, we performed immunofluorescence staining, and we found that the majority of the cells that were positive for miR-21 were also positive for fibroblast-specific protein (FSP)-1 (Figures 1C and 1D), but not α-smooth muscle cell actin (α-SMA) (Figures 1E and 1F), suggesting that miR-21 is in part upregulated by fibroblasts. Negative controls are shown in Figure S1.

The average staining of FSP-1 in the whole vessel wall was significantly elevated in stenotic tissue compared to controls (stenotic, 64.55 ± 9.59; control, 28.37 ± 8.12; average increase, 228%; $p = 0.034$; Figures S2A and S2C). We next determined the expression of FSP-1(+) cells in the intima and media + adventitia layers of the vessel wall. Semiquantitative analysis for FSP-1(+) cells indicated that there were significant increases in FSP-1(+) cells in the intima (stenotic, 52.58 ± 11.26; control, 15.05 ± 5.85; average increase, 349%; $p = 0.024$; Figure 1D) and media plus adventitia of the stenotic tissue when compared to controls (stenotic, 68.63 ± 7.43; control, 30.11 ± 8.69; average increase, 228%; $p = 0.023$; Figure 1D). Next, we determined whether the fibroblasts were the activated phenotype by immunostaining for fibroblast-activated protein (FAP) (Figures S2A and S2B). Interestingly, there was no significant difference in the average FAP index between both groups.

Then, semiquantitative analysis for α-SMA(+) cells was performed, and there were significant increases in the intima (stenotic, 44.51 ± 0.52; control, 15.54 ± 5.36; average increase, 286%; $p = 0.0064$) and media plus adventitia areas of the stenotic tissue when compared to controls (stenotic, 53.39 ± 12.90; control, 21.92 ± 3.24; average increase, 244%; $p = 0.04$). We next performed ISH for miR-21 followed by immunofluorescence staining, and we observed a minimal association of miR-21 expression and cells staining positive for CD31 and α-SMA (Figure S3). Consistent with increased miR-21 expression, there was a significant decrease in phosphatase and tensin homolog (PTEN), a downstream target gene of miR-21 staining in the

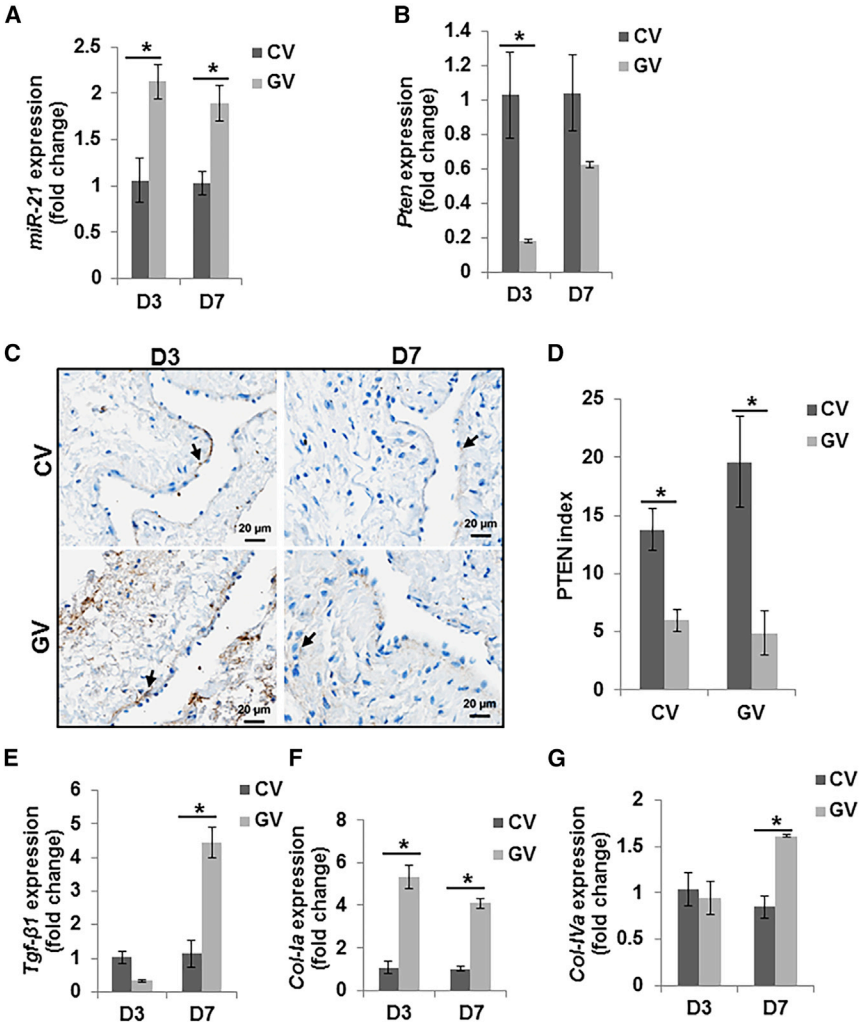

Figure 2. AVF Placement Induces miR-21 Expression while Suppressing PTEN and Increasing Profibrotic Genes in the Outflow Veins

Gene expression was assessed by qRT-PCR for (A) *miR-21* and (B) *Pten* in the outflow vein (GV) compared to the contralateral jugular vein (CV) at 3 days (D3) and 7 days (D7) after AVF placement. There was a significant increase in miR-21 expression at days 3 and 7 after AVF placement, with a significant decrease in *Pten* expression at 3 days after AVF creation. Tissue sections of the outflow veins of AVF were immunostained for (C) PTEN to assess miR-21 functionality and acquired at 20× magnification. Arrowheads identify cells staining positive for PTEN in (C). The mean intensity of the brown PTEN stain is presented as a bar graph (D), and there is a significant decrease in PTEN staining in GVs compared to CVs. Gene expression was assessed by qRT-PCR for (E) *Tgfβ-1*, (F) *Col-Ia*, and (G) *Col-IVa* in the outflow vein (GV) compared to the contralateral jugular vein (CV) at 3 days (D3) and 7 days (D7) after AVF placement. The gene expressions of *Tgfβ-1* and *Col-IVa* were significantly increased at day 7 in the GV compared to the CV. However, *Col-Ia* expression was significantly increased at days 3 and 7 in the GV compared to the CV. Each data point in the bar graph represents the mean ± SEM of 3 animals. Two-way ANOVA with Student's t test with Bonferroni correction was performed. Significant differences between CV and GV at the respective time points are indicated (*$p < 0.05$).

stenotic vessels (stenotic, 2.95 ± 0.68; control, 9.13 ± 1.21; average decrease, 68%; p = 0.0045; Figures 1G, 1H, and S4A) compared to controls.[8]

Cellular proliferation is a hallmark of venous stenotic tissue.[9,10] We performed Ki-67 staining to assess this, and we observed that there was a significant increase in the average Ki-67 index in the stenotic tissue compared to controls (stenotic, 50 ± 9.00; control, 31.32 ± 3.49; average increase, 162%; p = 0.048; Figures 1I, 1J, and S4B). Finally, terminal deoxynucleotidyl transferase dUTP nick-end labeling (TUNEL) staining was performed to assess whether there was a difference in the presence of apoptotic cells, and we observed that there was no significant difference in the average TUNEL index between both groups (data not shown).

AVF Creation Upregulated miR-21 Expression in the Outflow Veins of Murine AVFs

We performed qRT-PCR to assess the miR-21 expression in a murine model with chronic kidney disease (CKD) and AVF. The gene expression of miR-21 was significantly increased at 3 days after AVF placement in graft veins (GVs) compared to control veins (GV, 2.12 ± 0.13; CV, 1.06 ± 0.23; average increase, 200%; p = 0.016), and it remained significantly elevated at 7 days after AVF placement (GV, 1.89 ± 0.19; CV, 1.02 ± 0.17; average increase, 185%; p = 0.031; Figure 2A). The average *Pten* gene expression was significantly decreased in the GV compared to the CV at day 3 (GV, 0.18 ± 0.013; CV, 1.03 ± 0.25; average decrease, 82%; p = 0.015; Figure 2B).

Next, staining for PTEN (Figure 2C) was performed, and it demonstrated that there was a significant decrease in the GV compared to the CV at day 3 (GV, 5.99 ± 0.95; CV, 13.77 ± 3.93; average decrease, 56%; p = 0.019; Figure 2D) and day 7 (GV, 4.87 ± 1.92; CV, 19.59 ± 3.93; average decrease, 82%; p = 0.028). Surgical placement of the AVF induces a Hyp environment in the vessel wall of the GV caused by disruption of the microvascular network in the vessel wall. Hypoxic injury was assessed by immunohistochemistry for Hyp-inducible factor-1 alpha (Hif-1α; Figure S5A). AVF creation significantly increased the average Hif-1α staining at day 3 (GV, 14.13 ± 1.94; CV, 4.21 ± 0.73; average increase, 336%; p = 0.009; Figure S5B), and it remained significantly higher at day 7 in the GV compared to the CV (GV, 16.12 ± 1.67; CV, 3.61 ± 0.83; average decrease, 447%; p = 0.0046).

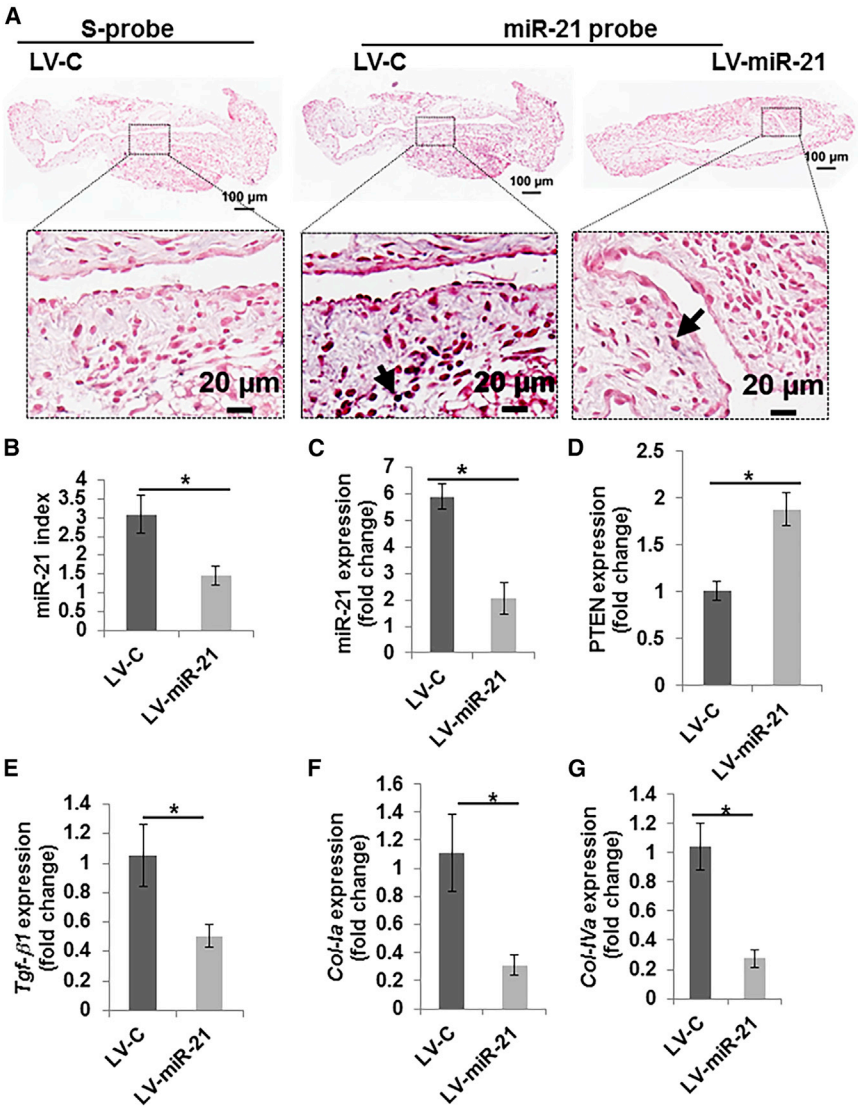

Figure 3. miR-21 Knockdown Shows Decreased Expressions of miR-21 and Profibrotic Genes in the AVF Outflow Veins

An arteriovenous fistula (AVF) was created, and 1×10^7 PFU lentivirus comprising shRNA targeting miR-21 (LV-miR-21) or scramble (LV-C) in 10 μL PBS were layered onto the adventitia of the outflow vein (GV) of the AVF. miR-21 expression was assessed by (A) *in situ* hybridization (ISH) and (C) qRT-PCR in GVs at 3 days after the AVF creation. (A) Representative 20× images were captured using a Zeiss microscope (upper panel), and areas enclosed by dashed boxes in the upper panels are digitally enlarged and shown in the lower panels. Arrowheads indicate the purple stain of miR-21 transcript, and the nucleus is stained red. ISH was also performed with scrambled miR probe (S-probe) to serve as the negative control. (B) The mean intensity of the purple stain is presented as a bar graph. There is a significant decrease in miR-21 expression at 3 days after LV-miR-21 transduction in the vessel wall compared to LV-C-transduced vessels. At 3 days after AVF creation, qRT-PCR was performed to assess the gene expressions of PTEN and profibrotic genes (D) *Pten,* (E) *Tgf-β1*, (F) *Col-Ia*, and (G) *Col-Iva* in GVs. The data were normalized to the gene expressions in the GVs of LV-C-transduced AVFs and expressed as mean fold change ± SEM of $n \geq 6$. There were significant decreases in the gene expressions of (D) *Pten*, (E) *Tgf-β1*, (F) *Col-Ia*, and (G) *Col-IVa* in LV-miR-21-transduced vessels compared to LV-C-transduced vessels. *$p < 0.05$.

AVF Creation Upregulated Profibrotic Genes in the GVs

miR-21 can upregulate genes involved in the *Tgf-β* pathway that can cause tissue fibrosis.[11] This prompted us to examine gene expression of profibrotic genes, including *Fsp-1*, *Tgf-β1*, matrix metalloprotease (*Mmp-2*), and *Col-Ia* in the GV at days 3 and 7 after AVF placement. There was a significant increase in *Fsp-1* expression in the GV compared to CV at day 7 after AVF creation (GV, 11.66 ± 2.19; CV, 1.16 ± 0.47; average increase, 1,006%; $p = 0.0016$; Figure S5C). In addition to these results, *Tgf-β*, *Mmp-2*, *Col-Ia*, and *Col-IVa* were significantly increased in the GV compared to CV at day 7 (*Tgf-β1* GV, 4.45 ± 0.45; CV, 1.13 ± 0.41; average increase, 393%; $p < 0.001$; Figure 2E; *Col-Ia* day 3 GV, 5.31 ± 0.56; CV, 1.07 ± 0.27; average increase, 495%; $p = 0.0008$; day 7 GV, 4.09 ± 0.23; CV, 1.016 ± 0.13; average increase, 402%; $p = 0.0016$; Figure 2F; *Col-IVa* day 7 GV, 41.61 ± 0.016; CV, 0.85 ± 0.12; average increase, 190%; $p = 0.022$; Figure 2G; and *Mmp-2* GV, 3.48 ± 0.38; CV, 1.04 ± 0.19; average increase, 334.7%; $p < 0.001$; Figure S5D). We speculate that the increase in TGF-β1 may occur due to the downregulation of SMAD7 by miR-21,[12] leading to the upregulation of *Col-Ia* at day 3.

Lentivirus-Mediated shRNA Transduction Blocks miR-21 Expression in the Outflow Vein of Murine AVFs

miR-21 knockdown in the outflow veins of AVFs was performed using a lentivirus that comprised shRNA that targeted the miR-21 gene (LV-miR-21) or control shRNA (LV-C), delivered to the adventitia of the outflow vein immediately after AVF creation (Figure 3A). *In situ* hybridization for miR-21 demonstrated that there was a significant decrease in the average miR-21 expression in the outflow veins transduced with LV-miR-21 compared to control vessels at 3 days after AVF creation (LV-miR-21, 1.45 ± 0.25; LV-C, 3.09 ± 0.50; average reduction, 53%; $p = 0.024$; Figure 3B). We observed that the vessels transduced with LV-miR-21 had a significant decrease in miR-21 expression at 3 days after AVF creation when compared to LV-C vessels (LV-miR-21, 2.07 ± 0.60; LV-C, 5.90 ± 0.48; average reduction, 65%; $p < 0.001$; Figure 3C). *In situ* hybridization followed by immunofluorescence staining for FSP-1 demonstrated that there was decreased miR-21 staining in the FSP-1(+) cells (Figure S6). Finally, we observed that the average gene expression of PTEN was significantly increased in the LV-miR-21-transduced vessels compared to control vessels

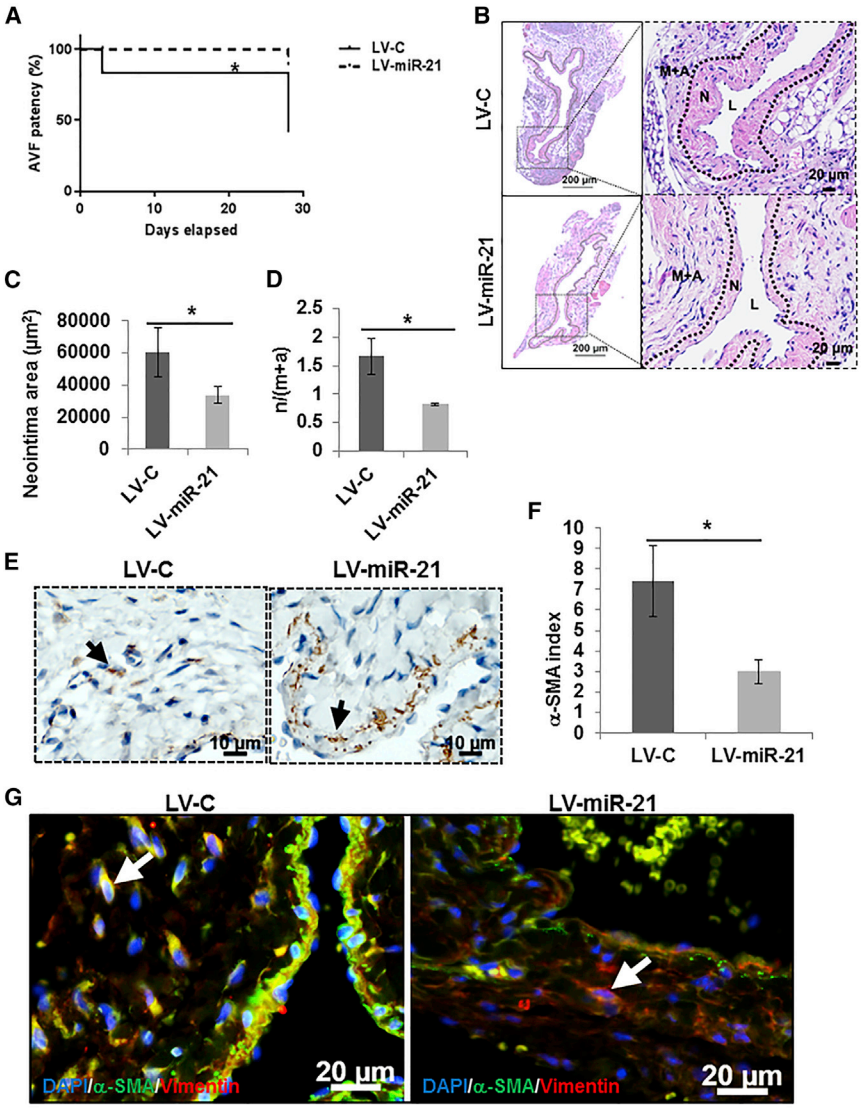

Figure 4. miR-21 Knockdown Vein Segments Have Improved AVF Patency with Reductions in Neointima Formation, Myofibroblasts, and Smooth Muscle Cell Accumulation in the Vessel Wall

An arteriovenous fistula (AVF) was created, and 1×10^7 PFU lentivirus comprising shRNA targeting miR-21 (LV-miR-21) or scramble (LV-C) in 10 μL PBS were layered onto the adventitia of the outflow vein (GV) of the AVF. (A) Kaplan-Meier estimates demonstrate that there was a significant improvement in AVF patency in the LV-miR-21-transduced vessels (dotted line) when compared to LV-C-transduced vessels (solid line) (log rank test, $p < 0.05$; $n \geq 6$ at each time point). Tissue sections of the GVs at day 28 of AVF creation were stained for H&E. (B) H&E staining areas enclosed by dashed boxes in the left panels (20×) are digitally enlarged and shown as right panels, where the lumen (*L*), neointima (*N*), and media plus adventitia (*M* + *A*) layers are separated by a dotted line. Histomorphometric analysis was performed using Zen Pro software to assess the areas of lumen, neointima, and media plus adventitia. There were significant reductions in (C) the neointima and (D) the ratio of neointima/media plus adventitia in LV-miR-21-transduced vessels compared to LV-C-transduced vessels. Tissue sections of the GVs at day 28 of AVF creation were immunostained for (A) α-SMA, and co-immunofluorescence staining was performed for (G) α-SMA and vimentin. The α-SMA(+) cells stained brown (arrowheads in E) were found to be more in the media of the LV-C group compared to the LV-miR-21 group, where α-SMA staining shows in the sub-endothelial layer (the entire tissue sections as low-magnification images are shown in Figure S8C). (F) The mean intensity of the chromogen staining (α-SMA index) was measured as described. (G) Representative co-immunofluorescence images of α-SMA (cells stained green), vimentin (red), and DAPI (blue) for nuclei. Cells staining positive for both α-SMA and vimentin (myofibroblasts indicated with arrowheads) are low in LV-miR-21-transduced GVs (C, right panel) compared to LV-C (C, left panel). The enlarged individual channels are shown in Figure S8. Each bar represents the mean ± SEM of $n \geq 6$ animals per group and the data points with an asterisk indicate $p < 0.05$.

(LV-miR-21, 6.34 ± 0.67; LV-C, 2.19 ± 0.71; average increase, 289%; p = 0.014; Figure 3D).

miR-21 Knockdown Abrogates Gene Expression of *TGF-β1*, *Col-Ia*, and *Col-IVa* in the GVs

We observed that there was a significant reduction in the expression of profibrotic genes *Tgf-β1* (LV-miR-21, 0.51 ± 0.078; C, 1.05 ± 0.21; average reduction, 52%; p = 0.021; Figure 3E), *Col-Ia* (LV-miR-21, 0.31 ± 0.07; C, 1.11 ± 0.27; average reduction, 72%; p = 0.039; Figure 3F), and *Col-IVa* (LV-miR-21, 0.28 ± 0.058; C, 1.04 ± 0.16; average reduction, 74%; p = 0.003; Figure 3G) in LV-miR-21-transduced vessels compared to controls. However, there was no significant difference in gene expression of FSP-1 and MMP-2 in LV-miR-21-treated vessels compared to LV-C-treated vessels at 3 days after AVF creation (data not shown).

Positive Vascular Remodeling Occurs with Loss of miR-21 in the GVs of AVFs

Vascular remodeling was determined by assessing the AVF patency and histomorphometric analysis after miR-21 knockdown in the outflow veins (LV-miR-21) or control shRNA (LV-C) delivered to the adventitia of the outflow vein immediately after AVF creation. We assessed the patency of the fistula, and we observed a significant increase in the patency of vessels transduced with LV-miR-21 compared to controls (log rank, p = 0.025; Figure 4A). Histomorphometric analysis demonstrated a significant decrease in the average neointima area of the LV-miR-21-transduced vessels compared to controls (LV-miR-21, 33,732.3 ± 3,408 μm^2; LV-C, 60,561 ± 15,169 μm^2; average reduction, 44%; p = 0.0051; Figures 4B and 4C), with a significant decrease in the mean ratio of neointima area to media plus adventitia area (LV-miR-21,

0.85 ± 0.022; LV-C, 1.95 ± 0.32; average reduction, 56%; p = 0.0058; Figure 4D).

miR-21 Knockdown Had No Impact on Serum Creatinine and BUN

It may be argued that uremia had a significant impact on vascular remodeling. We determined the serum blood urea nitrogen (BUN) and creatinine levels in both groups. There was no difference in the average serum BUN between both groups at day 3 (LV-miR-21, 66.2 ± 2.1 mg/dL; LV-C, 65.43 ± 1.35 mg/dL; p = 0.75) and at day 28 (LV-miR-21, 66.7 ± 2.96 mg/dL; LV-C, 66.4 ± 3.11 mg/dL; p = 0.75). In addition, there was no difference in the average serum creatinine levels between both groups at day 3 (LV-miR-21, 0.57 ± 0.03 mg/dL; LV-C, 0.5 ± 0.083 mg/dL; p = 0.56) and at day 28 (LV-miR-21, 0.62 ± 0.05 mg/dL; LV-C, 0.62 ± 0.084 mg/dL; p = 0.32).

LV-miR-21-Transduced Vessels Have Reduced Myofibroblast Staining

Immunostaining revealed that the majority of cells that stained positive for α-SMA were significantly decreased in LV-miR-21-transduced vessels compared to controls (LV-miR-21, 2.98 ± 0.57; LV-C, 7.40 ± 1.73; average reduction, 60%; p = 0.029; Figures 4F and 4G). Adjacent tissue sections were co-stained for both FSP-1 and α-SMA, and cells that were positive for FSP-1 were also positive for α-SMA in control vessels (Figures S7 and 4F), indicating the presence of myofibroblasts.

We next performed co-immunostaining for vimentin and α-SMA to determine if the α-SMA-positive cells were differentiating to synthetic myofibroblasts.[13] Cells that stained positive for α-SMA also co-stained for vimentin, and they were primarily located in the media and adventitia of the vessels transduced with LV-C (arrowhead, Figure 4H, left panel; the individual channels are shown in the upper panel of Figure S8). However, in LV-miR-21-transduced vessels, there was a decrease in cells staining positive for both α-SMA and vimentin (arrowhead, Figure 4H, right panel; Figure S8, lower panel). These data suggest that FSP-1(+) cells in the media and adventitia were differentiating into α-SMA(+) myofibroblasts and miR-21 knockdown was inhibiting the differentiation of FSP-1(+) cells to myofibroblasts in the GVs.

Hif-1α and pSMAD-2 and -3 Levels Are Decreased in LV-miR-21-Transduced Vessels

Several studies have demonstrated that there is cross-talk among Tgf-β1, miR-21, and Hyp,[11,14] and AVF creation can lead to the upregulation of Tgf-β1 and Hif-1α in outflow veins after AVF creation, as observed in the present study. Therefore, we sought to investigate whether LV-miR-21-transduced vessels would have decreased Hif-1α, phospho-SMAD2 (pSMAD-2), phospho-SMAD3 (pSMAD-3), and PTEN levels compared to controls.

Immunostaining of Hif-1α at 28 days after AVF creation demonstrated that there was a significant decrease in the average Hif-1α staining in the LV-miR-21-transduced vessels compared to controls (LV-miR-21, 4.41 ± 0.70; LV-C, 9.34 ± 1.05; average reduction, 53%; p = 0.007; Figures 5A, 5B, and S9A). The pSMAD2 index (LV-miR-21, 4.77 ± 1.62; LV-C, 10.31 ± 1.20; average reduction, 54%; p = 0.026; Figures 5C, 5D, and S9B) and the pSMAD3 index (LV-miR-21, 26.51 ± 1.67; LV-C, 39.77 ± 3.73; average reduction, 33%; p = 0.0057; Figures 5E, 5F, and S9C) were significantly decreased in the LV-miR-21-transduced vessels compared to controls. As expected, the average PTEN index was significantly increased in the vessels transduced with LV-miR-21 compared to controls (LV-miR-21, 6.34 ± 0.67; LV-C, 2.19 ± 0.71; average increase, 289%; p = 0.014; Figures 5G, 5H, and S9D). The representative low-magnification images of entire tissue sections are shown in Figure S9 (A, Hif-1α; B, pSMAD2; C, pSMAD3; and D, PTEN).

miR-21 Knockdown Increases Apoptosis and Decreases Cell Proliferation in GVs

TUNEL staining and Ki-67 staining were performed to assess the extent of apoptosis and cell proliferation in the vessels transduced with LV-miR-21 compared to controls. TUNEL staining was significantly increased in the LV-miR-21-transduced vessels compared to controls (LV-miR-21, 26.93 ± 2.34; LV-C, 12.94 ± 2.63; average increase, 208%; p = 0.0019; Figures 5I, 5J, and S9E). There was a significant decrease in the average Ki-67 staining in the vessels transduced with LV-miR-21 when compared to controls (LV-miR-21, 1.4 ± 0.3; LV-C, 4.13 ± 0.47; average decrease, 67%; p = 0.0006; Figures 5K, 5L, and S9F). The representative low-magnification images of entire tissue sections are shown in Figure S9 (E, TUNEL; and F, Ki-67).

Hypoxia Induces miR-21 Expression in Hypoxic Pulmonary Vein Fibroblasts

We took advantage of the observation that Hyp induces the differentiation of fibroblasts to α-SMA(+) cells.[2] Because we observed that HIF-1α staining was reduced in the LV-miR-21-transduced vessels and miR-21 expression was associated with fibroblasts, we investigated miR-21 gene expression in pulmonary vein fibroblasts subjected to Hyp. The average gene expression of miR-21 was significantly increased in the murine pulmonary vein fibroblasts when subjected to Hyp for 24 h compared to cells grown under normoxia (Nox) (Hyp, 2.39 ± 0.3; Nox, 1.02 ± 0.16; average increase, 233%; p = 0.016), and it remained significantly elevated at 48 h (Hyp, 2.18 ± 0.22; average increase, 213%; p = 0.014; Figure 6A).

miR-21 Knockdown Increases *Pten* with a Decrease in *Tgf-β1* Expression in Hypoxic Fibroblasts

We next determined the effect of loss of miR-21 function on fibroblast differentiation to α-SMA(+) cells under both Hyp and normoxic conditions. miR-21 knockdown in the fibroblasts was achieved by locked nucleic acid (LNA)-anti-miR-21 transfection. Under Hyp conditions, the average gene expression of miR-21 was significantly reduced in LNA-anti-miR-21-transfected (miR-21) fibroblasts compared to control LNA-transfected (C) fibroblasts, subjected to Hyp for 24 h (miR-21, 0.0018 ± 0.00067; C, 2.38 ± 0.30; average decrease, 99%; p = 0.0015; Figure 6B) and 48 h (miR-21, 0.032 ± 0.024; C, 2.18 ± 0.23;

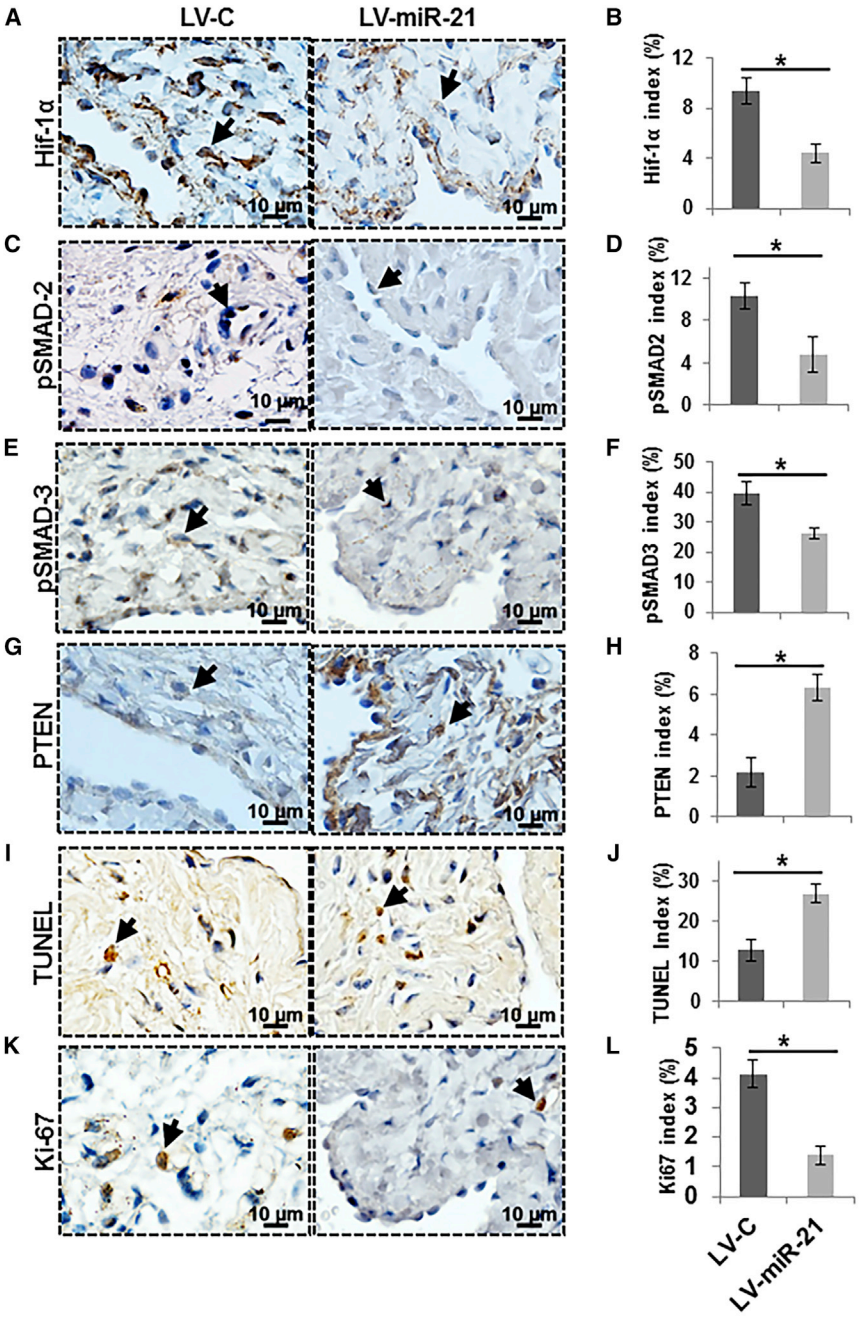

Figure 5. miR-21 Knockdown Vessels Have Shown Decreased Cells Staining Positive for Hif-1α, pSMAD2, pSMAD3, and Ki-67 and Increased PTEN and TUNEL

An arteriovenous fistula (AVF) was created and immediately layered with 1 × 10^7 PFU lentivirus comprised of a shRNA targeting miR-21 (LV-miR-21) or scramble (LV-C) in 10 μL PBS onto the outflow veins of AVFs. Tissue sections of the outflow veins of AVF were immunostained for (A) Hif-1α, (C) pSMAD2, (E) pSMAD3, (G) PTEN, (I) TUNEL, and (K) Ki-67. Representative complete images are shown in Figure S10. Arrowheads indicate the brown stain present in the nucleus for (A) Hif-1α, (B) pSMAD2, (E) pSMAD3, (I) TUNEL, and (K) Ki-67 and in the cytoplasm for (G) PTEN at 28 days after AVF placement. See Figure S9 for representative 20× images. The intensity of the brown stain is presented as a bar graph for (B) Hif-1α, (D) pSMAD2, (F) pSMAD3, (H) PTEN, (J) TUNEL, and (L) Ki-67. There were significant decreases in Hif-1α, pSMAD2, pSMAD3, and Ki-67 with significant increases in PTEN and TUNEL in LV-miR-21-transduced vessels compared to LV-C-transduced vessels. Each bar graph represents the mean ± SEM of n ≥ 6 animals per group. *p < 0.05.

average decrease, 99%; p = 0 0.0007). The average gene expression of *Pten* was significantly increased (Hyp-C, 35.77 ± 2.62; Nox-C, 1.01 ± 0.08; average increase, 3,553%; p < 0.0001; Figure 6C) in fibroblast cells exposed to Hyp compared to normoxia. However, *Pten* expression was significantly increased in miR-21-knockdown fibroblasts under Hyp (Hyp-miR-21, 137.03 ± 11.35; Hyp-C, 35.77 ± 2.62; average increase, 383%; p < 0.0001; Figure 6C) and normoxia conditions (Nox-miR-21, 26.13 ± 7.32; Nox-C, 1.01 ± 0.08; average increase, 2,596%; p = 0.025).

Finally, we determined the gene expression of *Tgf-β1* under similar conditions. The average gene expression of *Tgf-β1* was significantly increased in fibroblasts under Hyp conditions compared to normoxic conditions (Hyp-C, 2.23 ± 0.44; Nox-C, 1.04 ± 0.20; average increase, 214%; p < 0.0001; Figure 6D). Knockdown of miR-21 significantly decreased Hyp-induced *Tgf-β1* expression (Hyp-miR-21, 0.15 ± 0.065; Hyp-C, 2.23 ± 0.44; average decrease, 94%; p < 0.0001).

miR-21 Knockdown Abrogates Hypoxia-Induced Activation of pSMAD2 and pSMAD3 in Fibroblasts

Because TGF-β1 was significantly increased in Hyp fibroblasts, we decided to assess the phosphorylation of SMAD2 and -3. There was a significant increase in the phosphorylation of SMAD2 in cells exposed to Hyp compared to normoxia (pSMAD2 Hyp-C, 501.9% ± 11.47%; Nox-C, 100% ± 0.0%; average increase, 502%; p < 0.0001; Figures 7A and 7B) at 24 h. In addition, there was a significant increase in the phosphorylation of SMAD3 (Hyp-C, 502.06% ± 21.2%; Nox-C, 100% ± 0.0%; average increase, 502%; p < 0.0001; Figures 7A and 7C). However, Hyp fibroblasts that had reduced miR-21 gene expression had a significant decrease in both the pSMAD2 (Hyp-miR-21, 249.8% ± 3.15%; Hyp-C, 501.9% ± 11%; average reduction, 50%; p < 0.0001; Figures 7A and 7B) and pSMAD3 (Hyp-miR-21, 125.31% ± 37.37%; Hyp-C, 502.06% ± 21%; average reduction, 75%; p = 0.00095; Figures 7A and 7C) levels

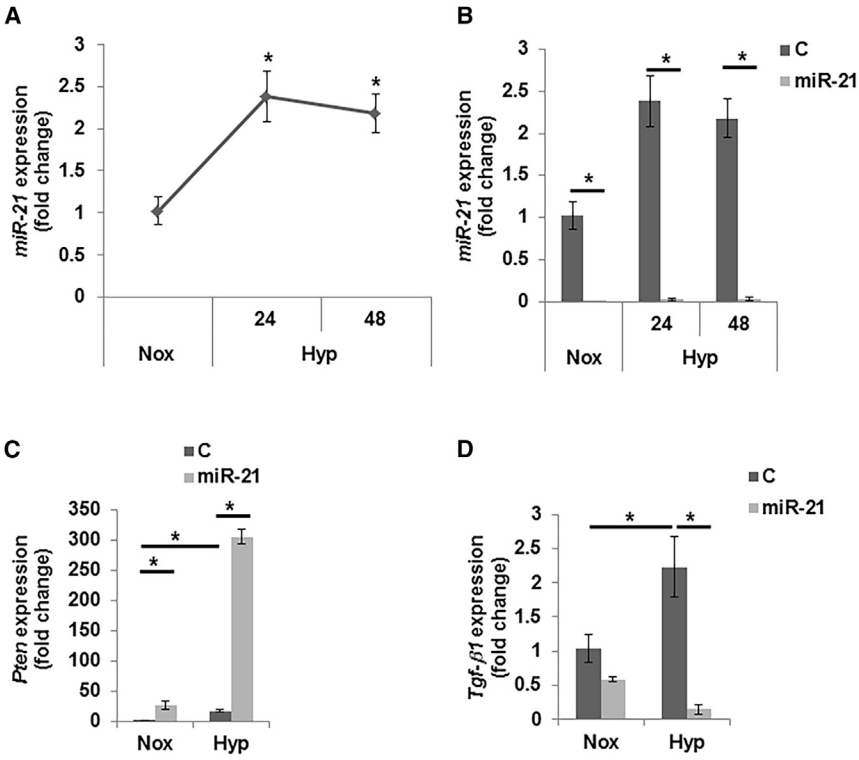

Figure 6. Hypoxia Upregulates the Gene Expression of miR-21 and Its Downstream Target Genes in Fibroblasts

Murine pulmonary vein fibroblasts were transfected with either LNA-Control (C) or LNA-anti-miR-21 (miR-21). After 24 h of transfection, cells were subjected to (1% O_2, 5% CO_2, and 94% air) hypoxia (Hyp), and gene expression was assessed by qRT-PCR. After transfection, cells cultured at regular conditions (95% air and 5% CO_2) were considered as normoxic (Nox) controls. (A) The gene expression of miR-21 was significantly increased in fibroblasts subjected to hypoxia for 24 and 48 h compared to normoxic cells. (B) miR-21 expression was significantly decreased in cells transfected with LNA-anti-miR-21 compared to hypoxic controls. Gene expressions of miR-21 target genes (C) *Pten* and (D) *Tgf-β1* were assessed under hypoxic and normoxic conditions. All data are normalized to normoxic fibroblasts (Nox) and 18S RNA as the reference gene except for miR-21 analysis where U6 RNA was used as a reference gene. Each bar graph represents mean ± SEM of three independent experiments per group. *p < 0.05.

compared to Hyp controls. These results suggest that miR-21 may function upstream of the Hyp-mediated activation of TGF-β1/SMAD signaling.

miR-21 Knockdown Increases PTEN and Protein Kinase B (AKT) Activation (pAKT) in Fibroblasts

Because the loss of miR-21 expression increased the PTEN gene expression in Hyp fibroblasts, we assessed the PTEN levels by performing western blotting (Figure 7A). Densitometric quantification of western blots revealed that the average protein expression of PTEN was significantly decreased by 48 h in Hyp cells compared to normoxic cells (Hyp-C, 71.6% ± 8.05%; Nox-C, 100% ± 0%; average decrease, 29%; p = 0.015; Figures 7A and 7D). However, there was a significant increase in PTEN levels in Hyp fibroblasts that had a knockdown of miR-21 compared to Hyp controls (Hyp-miR-21, 112.19% ± 9.63%; Hyp-C, 71.6% ± 8.05%; average increase, 156%; p = 0.03; Figure 7D).

PTEN is a known inhibitor of Pi3K/AKT signaling, and, therefore, we assessed AKT activation by performing western blotting for phospho-AKT (pAKT). There was a significant increase in the pAKT levels (Hyp, 190.7% ± 16.5%; Nox, 100% ± 0%; average increase, 191%; p = 0.0002) by 24 h, which remained significantly elevated at 48 h (Hyp, 174.43% ± 24.5%; Nox, 100% ± 0%; average increase, 174%; p = 0.0012; Figure 7E). However, there were decreased pAKT levels in both the Hyp and normoxic fibroblasts in which knockdown for miR-21 had been performed compared to controls at 24 h (Nox-miR-21, 49.24 ± 5.11; Nox-C, 100% ± 0%; average decrease, 50.7%; p = 0.00058; Hyp-miR-21, 54.19% ± 4.01%; Hyp-C, 190.7% ± 16.5%; average decrease, 72%; p = 0.0013) and at 48 h (Hyp-miR-21, 47.42% ± 3.04%; Hyp-C, 174.43% ± 24.5%; average decrease, 73%; p = 0.0068; Figure 7E).

miR-21 Knockdown Decreases Hypoxia-Induced Fibroblast Differentiation to Myofibroblasts

There was increased expression of α-SMA in fibroblasts subjected to Hyp compared to normoxia (Hyp-C, 129.2% ± 3.5%; Nox-C, 100% ± 0%; average increase, 129%; p = 0.001; Figures 8A and 8B). The α-SMA levels were significantly decreased in fibroblasts with knockdown for miR-21 when subjected to Hyp compared to controls (Hyp-miR-21, 36.19% ± 0.6%; Hyp-C, 129.2% ± 3.5%; average decrease, 72%; p < 0.0001; Figure 8B). Moreover, similar results were also observed under normoxic conditions (Nox-miR-21, 24.71% ± 3.56%; Nox-C, 100% ± 0%; average decrease, 75%; p < 0.0001; Figure 8B). To further confirm this observation, immunofluorescence staining for α-SMA and phalloidin was performed. Both α-SMA (Figure 8C) and phalloidin (Figure 8D) staining was increased in Hyp fibroblasts compared to normoxic fibroblasts. However, fibroblasts that had reduced miR-21 gene expression had a decrease in α-SMA (Figure 8C) and phalloidin staining under Hyp conditions compared to control (Figure 8D).

miR-21 Knockdown in Fibroblasts Causes an Increase in Apoptosis with No Change in Cell Proliferation

We investigated the extent of cell death and proliferation of fibroblasts subjected to Hyp and normoxia following miR-21 knockdown. The average caspase-3/7 activities were significantly increased in fibroblasts subjected to Hyp compared to normoxia (Hyp-C,

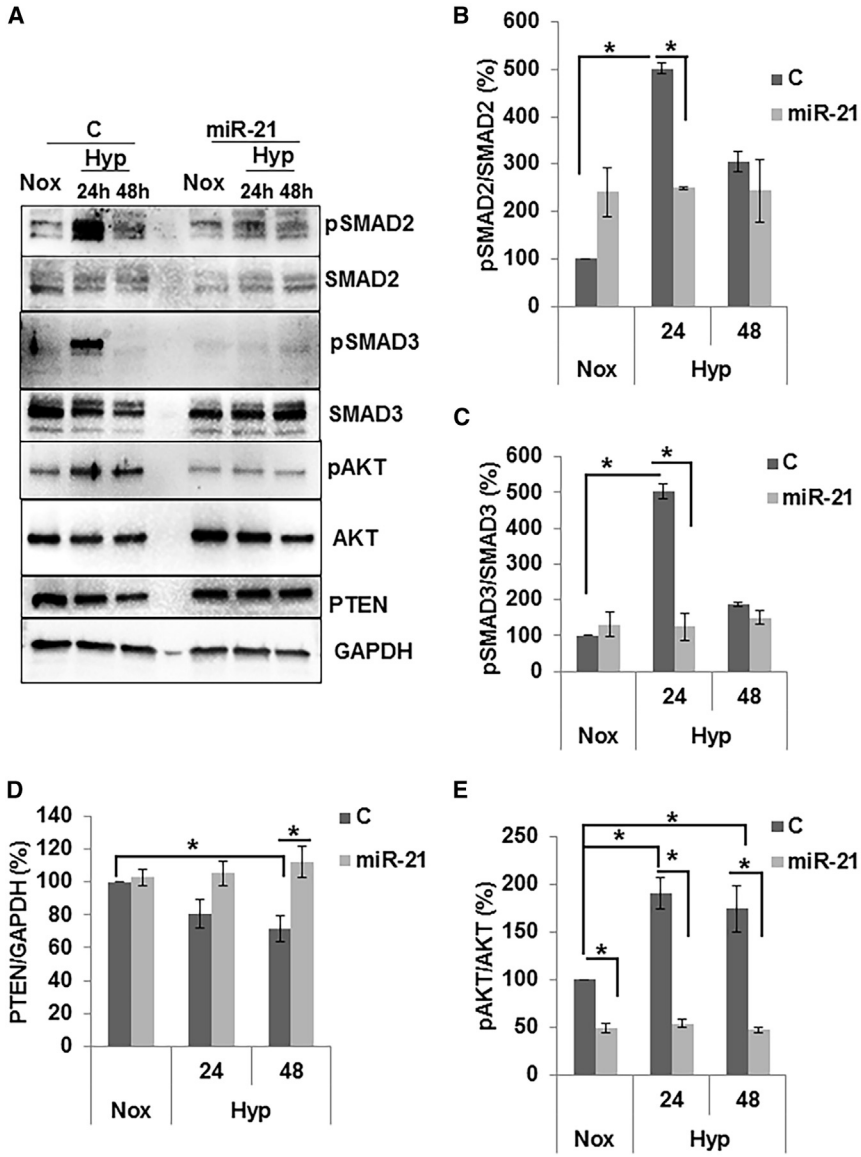

Figure 7. miR-21 Knockdown Abrogates Hypoxia-Induced pSMAD2/3 and AKT Signaling

Mouse pulmonary vein fibroblasts were transfected with either LNA-Control (C) or LNA-anti-miR-21 (miR-21). After 24 h of transfection, cells were subjected to (1% O_2, 5% CO_2, and 94% air) hypoxia (Hyp) for 24 and 48 h, and western blot was performed. After transfection, cells cultured at regular conditions (95% air and 5% CO_2) were considered as normoxic (Nox) controls. (A) Representative immunoblots for pSMAD2, SMAD2, pSMAD3, SMAD3, PTEN, pAKT, AKT, and GAPDH levels in fibroblasts subjected to 24 and 48 h of hypoxia or normoxia (n = 3). The band intensity of the western blots was quantified using NIH ImageJ software, and densitometric analysis was performed for (B) pSMAD2, (C) pSMAD3, (D) PTEN, and (E) pAKT. Each bar graph represents the mean ± SEM of three independent experiments per group.*p < 0.05.

DISCUSSION

In this study, we investigated the role of miR-21 in VNH associated with hemodialysis AVF vascular access failure. Increased expression of miR-21 has been demonstrated in fibrotic diseases[3] and coronary artery-to-vein bypass grafts in experimental murine and porcine models.[4] Here we demonstrated that there is increased gene expression of miR-21 in the outflow veins of experimental and clinical AVFs. Moreover, miR-21 expression was significantly increased in a murine AVF model in association with an increase in FSP-1 gene expression.

We next assessed the changes in miR-21 target genes; PTEN and TIMP-3, which are involved in cell survival and/or apoptosis, differentiation, and extracellular matrix deposition. In agreement with previous results, it was observed that there was decreased gene expression of PTEN, which is a downstream target of miR-21 at early time points of VNH progression. Extracellular matrix deposition and fibroblast accumulation are critical features observed in VNH.[15] Recent studies indicate that miR-21 and Tgf-β1 can be co-induced in tissue fibrosis[11] and miR-21 upregulation further enhances tissue fibrosis via the TGF-β1/pSMAD pathway.[14] Consistent with these observations, we observed that there is upregulation of genes involved in tissue fibrosis and matrix deposition, including collagens Ia and IVa and Tgf-β1 at day 7 after AVF creation. These results indicate that upregulation of miR-21 plays a significant role in AVF failure due to VNH.

When miR-21 was transduced in the outflow vein of AVFs in mice with CKD, there was a significant reduction in the N/M + A ratio with improved vascular access patency (Figure S10). Hypoxic fibroblasts with knockdown of miR-21 had decreased expressions of

120.64% ± 3.9%; Nox-C, 100% ± 2.8%; average increase, 121%; p = 0.0028; Figure 8E). However, loss of miR-21 increased the mean caspase-3/7 activity significantly in both normoxic fibroblasts (Nox-miR-21, 154.9% ± 5.9%; Nox-C, 100% ± 2.8%; average increase, 155%; p < 0.0001; Figure 8E) and Hyp fibroblasts (Hyp-miR-21, 135.1% ± 4.7%; Hyp-C, 120.6% ± 3.9%; average increase, 115%; p = 0.03; Figure 8E) compared to controls.

When we evaluated proliferation, we observed that, in Hyp fibroblasts, there was no significant difference in proliferation when compared to normoxic fibroblasts. However, proliferation was significantly increased in fibroblasts with knockdown of miR-21 under normoxic conditions (C, 100% ± 5.1%; miR-21, 127.02% ± 3.0%; average increase, 127%; p < 0.0001), but there was no significant difference in proliferation of Hyp fibroblasts compared to controls (Figure 8F).

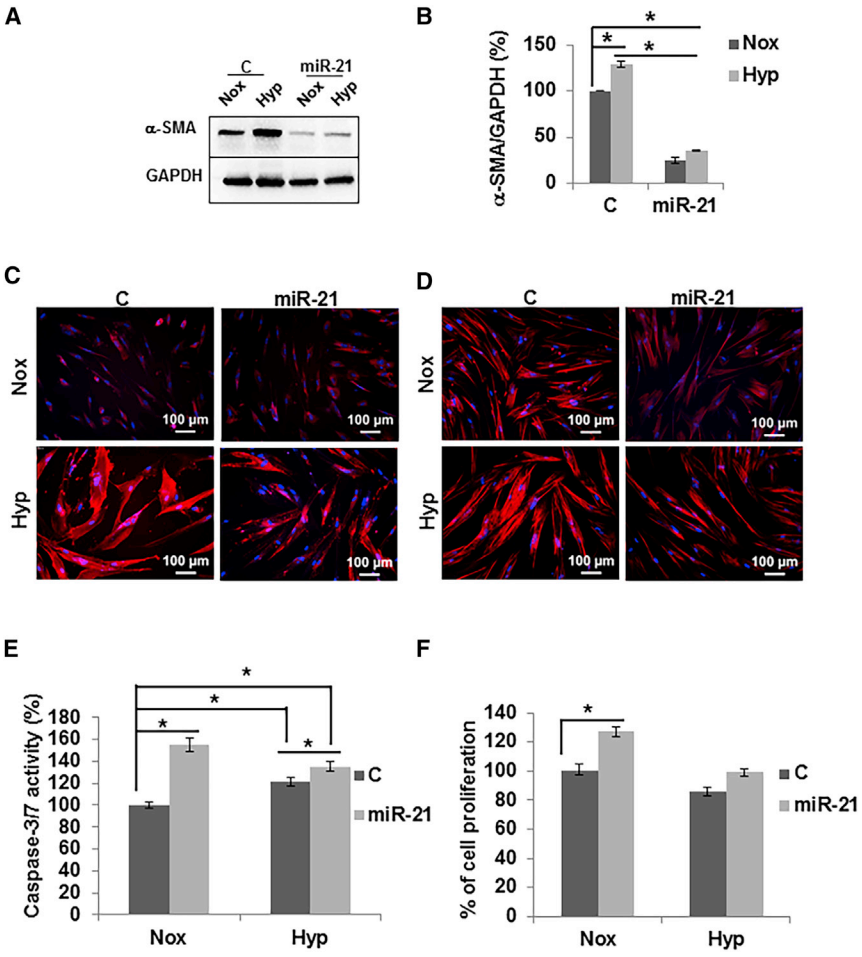

Figure 8. miR-21 Knockdown Abrogates Hypoxia-Induced Fibroblast-to-Myofibroblast Differentiation with an Increase in Apoptosis

Murine pulmonary vein fibroblasts were transfected with either LNA-Control (C) or LNA-anti-miR-21 (miR-21). After 24 h of transfection, cells were subjected to (1% O_2, 5% CO_2, and 94% air) hypoxia (Hyp) for 24 h, and western blot was performed. After transfection, cells cultured at regular conditions (95% air and 5% CO_2) were considered as normoxic (Nox) controls. Representative immunoblot for α-SMA (n = 3) at 24 h of hypoxia (A) with densitometric analysis and normalized to GAPDH for loading control (B). Immunofluorescence staining for α-SMA (C, red) and phalloidin (D, red) and nuclei stained for DAPI (blue). Images (10× magnification) presented are representative of 6 different fields of two independent experiments. (E) Apoptosis was assessed by caspase-3/7 activity and (F) cell proliferation was assessed as described. There was a significant increase in caspase-3/7 activity in LNA-miR-21-transfected cells. However, a significant increase in proliferation was observed only in normoxic cells with knockdown for miR-21. Each data point in the bar graph represents the mean ± SEM of three independent experiments per group. *$p < 0.05$.

TGF-β1, pSMAD2, pSMAD3, and pAKT with an increase in PTEN and a decrease in α-SMA with an increase in caspase-3/7 activity. Finally, we observed that there was increased gene expression of miR-21 in stenotic veins of AVFs removed from patients, and this was associated with fibroblasts in the vessel wall. *In situ* hybridization results revealed that miR-21 expression was predominantly localized in the intima and media layers, where cells abundantly stained for FSP-1 in the outflow veins of patients with failed AVF.

Histomorphometric analysis of outflow veins that had been transduced with lentivirus comprising shRNA to block miR-21 expression had significant reductions in neointima area and neointima/media plus adventitia and an increase in fistula patency compared to controls. Histological observations of the miR-21-knockdown vessels at day 28 of AVF creation indicated that there was a significant decrease in the α-SMA index despite no change in FSP-1 positive cells. Previous results demonstrated that there is increased FSP-1 staining by day 7 and α-SMA at day 28 after AVF creation in a murine model.[14] Moreover, co-immunostaining for vimentin and α-SMA revealed that the majority of α-SMA-positive cells localized in the media and adventitia were also positive for vimentin, suggesting that the smooth muscle cells are of the synthetic phenotype.[8] However, LV-miR-21-transduced vessels had fewer cells positive for α-SMA staining in the media and adventitial layers compared to controls. These results led us to speculate that the loss of miR-21 attenuated fibroblast-to-myofibroblast differentiation. Furthermore, LV-miR-21-transduced vessels had decreases in pSMAD2 and pSMAD3 levels, as an indication of decreased TGF-β/SMAD signaling in the outflow veins of mouse AVFs, with an increase in PTEN levels. In aggregate, these data suggest that miR-21 upregulation following AVF creation leads to the differentiation of fibroblasts to α-SMA-positive myofibroblasts and the attainment of a synthetic phenotype during VNH progression.

The increase in cell proliferation and decrease in apoptosis have been addressed in AVF failure. In addition, a decrease in cell proliferation with an increase in apoptosis was observed in the GVs of AVFs transduced with LV-miR-21 compared to LV-C at day 28 of AVF creation. However, the loss of miR-21 had no impact on cell proliferation, but it did result in an increase in apoptosis of fibroblasts when subjected to Hyp. Subtle changes in cell proliferation and apoptosis could be attributed to the increase in PTEN, a known inhibitor of cell survival associated with the loss of miR-21 in the vessel walls.[16]

The surgical procedure causes microvascular injury to the vessel wall, leading to Hyp, and Hyp can trigger proliferation, migration, and differentiation of fibroblasts and vascular smooth muscle cells and matrix deposition.[17] We investigated the role of miR-21 in Hyp-induced

fibroblast differentiation to myofibroblasts following a loss of function. Our results indicate that the loss of miR-21 abrogates Hyp-mediated TGF-β1 upregulation along with activation of pSMAD2 and -3, AKT activation, and α-SMA elevation in fibroblasts. In agreement with these results, sustained AKT activation is necessary for TGF-β1-mediated fibroblast-to-myofibroblast differentiation.[18] Furthermore, miR-21 suppresses PTEN expression that facilitates constitutive activation of the Pi3K/AKT pathway.[19] Together, these results confirm that miR-21 enhances Hyp-induced TGF-β1/SMAD signaling and fibroblast-to-myofibroblast differentiation (Figure S10). Moreover, miR-21 upregulated HIF-1α expression, and miR-21 and HIF-1α can function together as a feedback loop in exacerbating intracellular Hyp signaling.[4,20,21] Furthermore, miR-21 has also been implicated in causing an increase in smooth muscle cell migration via the modulation of tropomyosin-1 in an atherosclerosis murine model.[4]

In summary, our study identifies an important role of miR-21 reduction in improving vascular remodeling, with a decrease in profibrotic genes and an increase in vascular patency. At the cellular level, vascular remodeling effects seem to be mediated in part by fibroblast-to-myofibroblast differentiation. However, further studies utilizing cell-specific miR-21 loss-of and gain-of-function models need to be performed to decipher the cell-specific role of miR-21 as a potential target in treating VNH in AVF failure.

MATERIALS AND METHODS

Materials

All supplies for cell culture studies were obtained from Thermo Fisher Scientific (Waltham, MA, USA) unless otherwise stated. Mouse pulmonary vein fibroblasts (Cat# C57-6078) and fibroblast culture media (Cat# M2267) were purchased from Cell Biologics (Chicago, IL, USA). shRNA targeting miR-21 and scramble controls were a kind gift from professor Min-Hua Luo, China,[5] and the lentivirus was produced in HEK293T cells (ATCC, Cat# CRL-11268, Manassas, VA, USA), as described previously.[19] LNA-anti-miR-21 (Cat # YI04100688) and LNA scrambled control (Cat # YI00199006) were obtained from QIAGEN (Germantown, MD, USA). All histology supplies, including buffers and blocking reagents, were obtained from Dako Agilent (Santa Clara, CA, USA), unless otherwise stated.

Human Tissue Sections

Unstained tissue sections of the outflow veins of functional and failed AVFs from patients who were on hemodialysis were obtained from Dr. Padron Vazquez at the University of Miami Miller School of Medicine (Miami, FL, USA) and Dr. Chin-Wien Wu at the National Taiwan University Hospital (Hsinchu, Taiwan), with institutional review board (IRB) approval.[6,7]

In Situ Hybridization

In situ hybridization for miR-21 expression and localization in outflow veins of AVFs excised from the patients was performed using the miR-21 ISH kit (Exiqon A/S, Cat# 90002, Vedbaek, Denmark), according to the manufacturer's protocol.

Animal Experiments

All animal experiments were pre-approved by the Mayo Clinic Institutional Animal Care and Use Committee. C57BL/6J, 6- to 8-week-old male mice (Jackson Laboratory, Bar Harbor, ME, USA) were housed at 22°C temperature, 41% relative humidity, 12-h light-dark cycles, with access to food and water *ad libitum* prior to the experiments.

CKD Mice with AVF Creation

Mice were anesthetized with a ketamine (100 mg/kg body weight) and xylazine (10 mg/kg body weight) mixture prior to surgery, and nephrectomy was performed to create CKD as described.[10,17,22–24] The mice undergoing this procedure have been shown to have elevated BUN and creatinine by 3–4 weeks after nephrectomy.[10,17,22–24] After 28 days of CKD creation, the left carotid artery was connected to the left jugular vein to create an AVF as described.[22] The outflow vein of the fistula, also referred to as the GV, and the contralateral jugular vein (CV) of the same mouse as the control vein were excised for PCR at days 3 and 7 of fistula creation. The comparison of change in gene expression in CV and GV at each time point would not only be due to AVF creation but also to avoid the contribution of uremia.

For *in vivo* gene-knockdown studies, 1×10^7 plaque-forming units (PFU) lentivirus particles composed of miR-21 (LV-miR-21) or scrambled (LV-C) shRNA in 10 μL PBS was layered onto the adventitia of the GVs immediately after AVF creation.[10,22,24] The tissue samples were harvested on day 3 for gene expression analysis and on day 28 for histology analysis. The AVF patency was assessed immediately after AVF creation and at the time of tissue harvesting, as described previously.[2]

Serum Creatinine and Blood Urea Levels

Serum creatinine and BUN were measured at days 3 and 28 after AVF creation with lentivirus administration, using a serum creatinine colorimetric assay kit (700460, Cayman Chemicals, Ann Arbor, MI, USA) and a QuantiChrome urea assay kit (DIUR-100, BioAssay Systems, Hayward, CA, USA).

Immunohistochemistry and Morphometric Analysis

Paraffin-embedded GV tissues sections were stained with H&E, and then morphometric analysis was performed as described.[25] Sections were immunostained using primary antibody. Antibodies, suppliers, and dilutions are listed in Table 1. Non-specific control immunoglobulin G (IgG) staining was also performed with normal Rabbit IgG or mouse IgGs as primary antibody to serve as the negative control (Figures S1A and S1B). All images were captured at 20× objective using a Zeiss Axio Imager-M2 equipped with a Zeiss Axiocam 503 Color camera (Zeiss, Oberkochen, Germany) and a motorized stage. Vessel lumen area, vessel wall thickness, and intensity of chromogen stain were assessed by Zen-Pro software (Zeiss) as described.[22]

TUNEL Staining

Apoptosis was assessed by performing TUNEL staining on paraffin-embedded sections using a colorimetric TUNEL kit (R&D Systems,

Table 1. Characteristics of the Study Participants

Patient Characteristic	Control (n = 9)	Stenotic (n = 6)	Significance (p Value)
Age (years, mean ± SE)	68 ± 3.95	63.25 ± 9.0	0.58
Gender	5 M, 4 F	3 M, 3 F	0.45
Hypertension (%)	44.44	50	0.43
Diabetes (%)	55.56	50	0.71
Active smoker (%)	0	0	–
Dyslipidemia (%)	44.44	50	0.43
CAD (%)	44.44	25	0.45
Aspirin (%)	66.66	75	0.45
ACEI/ARB (%)	22.22	0	0.51
Statins (%)	22.22	0	0.32

M, male; F, female; CAD, coronary artery disease; ACEI/ARB, angiotensin-converting enzyme/angiotensinogen receptor blocker.

Cat# 4828-30-K, Minneapolis, MN, USA), according to the manufacturer's instructions.

RNA Isolation and Real-Time PCR Analysis

RNA was isolated using the miRNeasy Kit (QIAGEN, Germantown, MD, USA). cDNA was prepared using the i-script cDNA synthesis kit (Bio-Rad, Hercules, CA, USA), and real-time qPCR was performed using the iTaq universal SYBR green super mix (Bio-Rad) in a CFX5 thermal cycler (Bio-Rad), except for miR-21 analysis. All primers used for gene expression analysis are listed in Table S1. For miR-21 analysis, cDNA was prepared using TaqMan MicroRNA Reverse Transcription Kit (Applied Biosystems, Carlsbad, CA, USA), and gene expression was assessed using the miR-21 TaqMan assay (Applied Biosystems, Cat# 000397) and U6 microRNA (miRNA) (Applied Biosystems, Cat# 001973) as the internal reference gene. All gene expression data were normalized to respective CVs and expressed as fold change above the gene expression in the CVs, calculated according to the $2^{-\Delta\Delta CT}$ method.

Cell Culture

We purchased 3 vials of cells from the manufacturer at different time points (Cell Biologics, C57-6078). These cells were isolated from C57BL/6 mice. We used passage 4 of the cells to perform the experiments. The cells were from the same lot number. Experiments from these cells were performed in triplicate. For miR-21-knockdown experiments, cells in 10-cm dishes were transfected with either 5 μM control or LNA-miR-21 in opti-MEM using FuGENE HD (Roche, Indianapolis, IN, USA), following the manufacturer's protocol. After 24 h, cells were re-plated for experiments as described.

Caspase-3/7 Assay

Caspase-3/7 activity was measured using the Caspase-Glo 3/7 Assay (Promega, Madison, WI, USA), following the manufacturer's protocol.

Cell Proliferation

Cell proliferation was assessed using the CellTiter 96 Aqueous One Solution Cell Proliferation Assay System (Promega, Madison, WI, USA).

Western Blot

The lysates were resolved in 4%–20% SDS-PAGE followed by western blotting. The antibodies used for western blotting are listed in Table S2.

Statistical Methods

Data are expressed as mean ± SEM. Two-way ANOVA followed by Student's t test with post hoc Bonferroni correction was performed using JMP Pro 10 software (SAS, Cary, NC, USA). Significant differences between groups are indicated (*$p < 0.05$).

SUPPLEMENTAL INFORMATION

Supplemental Information can be found online at https://doi.org/10.1016/j.ymthe.2019.06.011.

AUTHOR CONTRIBUTIONS

S.K. and S.M. designed the entire study. S.K. performed a significant portion of the experiments. C.C. and C.Z. performed the animal surgeries. A.S. and M.S. contributed to the immunohistochemical analyses. E.C. and L.M. contributed to the ISH analysis. C.-C.W. and H.-L.S. contributed to the patient studies. S.K., S.M., and L.M. contributed to data organization and discussion. S.K. and S.M. wrote the paper.

CONFLICTS OF INTEREST

The authors declare no competing interests.

ACKNOWLEDGMENTS

We thank professor Min-Hua Luo, Center for Molecular Virology, Wuhan Institute of Virology, Chinese Academy of Sciences, China, for the generous gift of miR-21 and control shRNA construct. The authors acknowledge the assistance of Lucy Bahn, PhD, with editing this manuscript. This work was funded by NIH R01 grants to S.M. (HL098967 and DK107870) and a pilot grant from the Society of Interventional Radiology Foundation to S.K.

REFERENCES

1. Rooijens, P.P.G.M., Tordoir, J.H., Stijnen, T., Burgmans, J.P., Smet de, A.A., and Yo, T.I. (2004). Radiocephalic wrist arteriovenous fistula for hemodialysis: meta-analysis indicates a high primary failure rate. Eur. J. Vasc. Endovasc. Surg. *28*, 583–589.

2. Misra, S., Fu, A.A., Misra, K.D., Shergill, U.M., Leof, E.B., and Mukhopadhyay, D. (2010). Hypoxia-induced phenotypic switch of fibroblasts to myofibroblasts through a matrix metalloproteinase 2/tissue inhibitor of metalloproteinase-mediated pathway: implications for venous neointimal hyperplasia in hemodialysis access. J. Vasc. Interv. Radiol. *21*, 896–902.

3. Liu, G., Friggeri, A., Yang, Y., Milosevic, J., Ding, Q., Thannickal, V.J., Kaminski, N., and Abraham, E. (2010). miR-21 mediates fibrogenic activation of pulmonary fibroblasts and lung fibrosis. J. Exp. Med. *207*, 1589–1597.

4. McDonald, R.A., White, K.M., Wu, J., Cooley, B.C., Robertson, K.E., Halliday, C.A., McClure, J.D., Francis, S., Lu, R., Kennedy, S., et al. (2013). miRNA-21 is dysregulated

in response to vein grafting in multiple models and genetic ablation in mice attenuates neointima formation. Eur. Heart J. *34*, 1636–1643.

5. Fu, Y.R., Liu, X.J., Li, X.J., Shen, Z.Z., Yang, B., Wu, C.C., Li, J.F., Miao, L.F., Ye, H.Q., Qiao, G.H., et al. (2015). MicroRNA miR-21 attenuates human cytomegalovirus replication in neural cells by targeting Cdc25a. J. Virol. *89*, 1070–1082.
6. Tabbara, M., Duque, J.C., Martinez, L., Escobar, L.A., Wu, W., Pan, Y., Fernandez, N., Velazquez, O.C., Jaimes, E.A., Salman, L.H., and Vazquez-Padron, R.I. (2016). Preexisting and Postoperative Intimal Hyperplasia and Arteriovenous Fistula Outcomes. Am. J. Kidney Dis. *68*, 455–464.
7. Wu, C.C., Chen, L.J., Hsieh, M.Y., Lo, C.M., Lin, M.H., Tsai, H.E., Song, H.L., and Chiu, J.J. (2018). MicroRNA-21 and Venous Neointimal Hyperplasia of Dialysis Vascular Access. Clin. J. Am. Soc. Nephrol. *13*, 1712–1720.
8. Buscaglia, L.E., and Li, Y. (2011). Apoptosis and the target genes of microRNA-21. Chin. J. Cancer *30*, 371–380.
9. Roy-Chaudhury, P., Kelly, B.S., Miller, M.A., Reaves, A., Armstrong, J., Nanayakkara, N., and Heffelfinger, S.C. (2001). Venous neointimal hyperplasia in polytetrafluoroethylene dialysis grafts. Kidney Int. *59*, 2325–2334.
10. Yang, B., Janardhanan, R., Vohra, P., Greene, E.L., Bhattacharya, S., Withers, S., Roy, B., Nieves Torres, E.C., Mandrekar, J., Leof, E.B., et al. (2014). Adventitial transduction of lentivirus-shRNA-VEGF-A in arteriovenous fistula reduces venous stenosis formation. Kidney Int. *85*, 289–306.
11. Meng, X.M., Nikolic-Paterson, D.J., and Lan, H.Y. (2016). TGF-β: the master regulator of fibrosis. Nat. Rev. Nephrol. *12*, 325–338.
12. Li, S., Liu, W., Lei, Y., and Long, J. (2016). Regulatory effects of electronic beam irradiation on mir-21/smad7-mediated collagen I synthesis in keloid-derived fibroblasts. Biol. Open *5*, 1567–1574.
13. Lee, T., and Roy-Chaudhury, P. (2009). Advances and new frontiers in the pathophysiology of venous neointimal hyperplasia and dialysis access stenosis. Adv. Chronic Kidney Dis. *16*, 329–338.
14. Ardite, E., Perdiguero, E., Vidal, B., Gutarra, S., Serrano, A.L., and Muñoz-Cánoves, P. (2012). PAI-1-regulated miR-21 defines a novel age-associated fibrogenic pathway in muscular dystrophy. J. Cell Biol. *196*, 163–175.
15. Yang, B., Kilari, S., Brahmbhatt, A., McCall, D.L., Torres, E.N., Leof, E.B., Mukhopadhyay, D., and Misra, S. (2017). CorMatrix Wrapped Around the Adventitia of the Arteriovenous Fistula Outflow Vein Attenuates Venous Neointimal Hyperplasia. Sci. Rep. *7*, 14298.
16. Gao, Y., Chu, M., Hong, J., Shang, J., and Xu, D. (2014). Hypoxia induces cardiac fibroblast proliferation and phenotypic switch: a role for caveolae and caveolin-1/PTEN mediated pathway. J. Thorac. Dis. *6*, 1458–1468.
17. Misra, S., Shergill, U., Yang, B., Janardhanan, R., and Misra, K.D. (2010). Increased expression of HIF-1alpha, VEGF-A and its receptors, MMP-2, TIMP-1, and ADAMTS-1 at the venous stenosis of arteriovenous fistula in a mouse model with renal insufficiency. J. Vasc. Interv. Radiol. *21*, 1255–1261.
18. Kendall, R.T., and Feghali-Bostwick, C.A. (2014). Fibroblasts in fibrosis: novel roles and mediators. Front. Pharmacol. *5*, 123.
19. Kilari, S., Cossette, S., Pooya, S., Bordas, M., Huang, Y.W., Ramchandran, R., and Wilkinson, G.A. (2015). Endothelial Cell Surface Expressed Chemotaxis and Apoptosis Regulator (ECSCR) Regulates Lipolysis in White Adipocytes via the PTEN/AKT Signaling Pathway. PLoS ONE *10*, e0144185.
20. Liu, L.Z., Li, C., Chen, Q., Jing, Y., Carpenter, R., Jiang, Y., Kung, H.F., Lai, L., and Jiang, B.H. (2011). MiR-21 induced angiogenesis through AKT and ERK activation and HIF-1α expression. PLoS ONE *6*, e19139.
21. Liu, Y., Nie, H., Zhang, K., Ma, D., Yang, G., Zheng, Z., Liu, K., Yu, B., Zhai, C., and Yang, S. (2014). A feedback regulatory loop between HIF-1α and miR-21 in response to hypoxia in cardiomyocytes. FEBS Lett. *588*, 3137–3146.
22. Janardhanan, R., Yang, B., Kilari, S., Leof, E.B., Mukhopadhyay, D., and Misra, S. (2016). The Role of Repeat Administration of Adventitial Delivery of Lentivirus-shRNA-Vegf-A in Arteriovenous Fistula to Prevent Venous Stenosis Formation. J. Vasc. Interv. Radiol. *27*, 576–583.
23. Janardhanan, R., Yang, B., Vohra, P., Roy, B., Withers, S., Bhattacharya, S., Mandrekar, J., Kong, H., Leof, E.B., Mukhopadhyay, D., and Misra, S. (2013). Simvastatin reduces venous stenosis formation in a murine hemodialysis vascular access model. Kidney Int. *84*, 338–352.
24. Nieves Torres, E.C., Yang, B., Roy, B., Janardhanan, R., Brahmbhatt, A., Leof, E., Mukhopadhyay, D., and Misra, S. (2014). Adventitial delivery of lentivirus-shRNA-ADAMTS-1 reduces venous stenosis formation in arteriovenous fistula. PLoS ONE *9*, e94510.
25. Kilari, S., Yang, B., Sharma, A., McCall, D.L., and Misra, S. (2018). Increased transforming growth factor beta (TGF-β) and pSMAD3 signaling in a Murine Model for Contrast Induced Kidney Injury. Sci. Rep. *8*, 6630.